Negative-Mass Instability of the Spin and Motion of an Atomic Gas Driven by Optical Cavity Backaction

Jonathan Kohler, Justin A. Gerber, Emma Dowd, and Dan M. Stamper-Kurn

Negative-mass instability of the spin and motion of an atomic gas driven by optical cavity backaction

Jonathan Kohler,[1, *] Justin A. Gerber,[1] Emma Dowd,[1] and Dan M. Stamper-Kurn[1, 2, †]

[1]*Department of Physics, University of California, Berkeley, California 94720, USA*
[2]*Materials Sciences Division, Lawrence Berkeley National Laboratory, Berkeley, California 94720, USA*

We realize a spin-orbit interaction between the collective spin precession and center-of-mass motion of a trapped ultracold atomic gas, mediated by spin- and position-dependent dispersive coupling to a driven optical cavity. The collective spin, precessing near its highest-energy state in an applied magnetic field, can be approximated as a negative-mass harmonic oscillator. When the Larmor precession and mechanical motion are nearly resonant, cavity mediated coupling leads to a negative-mass instability, driving exponential growth of a correlated mode of the hybrid system. We observe this growth imprinted on modulations of the cavity field and estimate the full covariance of the resulting two-mode state by observing its transient decay during subsequent free evolution.

The description of a harmonic oscillator with negative mass applies to collective excitations in diverse non-equilibrium systems, such as solid-state crystals [1], plasmas [2, 3], superfluids [4], and cold atomic gases [5, 6]. The total Hamiltonian describing a negative-mass harmonic oscillator has the opposite sign of that of a positive-mass oscillator, resulting in an inverted energy spectrum, where an increased oscillation amplitude lowers the total energy. When a negative-mass oscillator is coherently coupled to a positive-mass oscillator at nearly the same frequency, the two-oscillator system can undergo an instability, where the transfer of energy between them leads to unbounded growth of the amplitudes of both oscillators. This negative-mass instability has been observed in the classical mechanics of trapped plasmas [7] and ion traps [8], and has been suggested to play a role in galactic structure [9].

Negative-mass oscillators also play an important role in quantum science. Glauber proposed that a negative-mass oscillator coupled to a zero-temperature bath would, through the negative-mass instability, function as an ideal quantum amplifier [10]. Joint measurement of resonant, but uncoupled, positive- and negative-mass oscillators allows for continuous measurement in a back-action-free subspace [11, 12], recently demonstrated [13, 14] as a method to circumvent standard quantum limits for position and force detection. Weak coupling of such modes, below the instability threshold, has been proposed for generation of steady-state, two-mode entanglement [15].

In this Letter, we report experimental realization of the negative-mass instability in a fully quantum, optodynamical system. Following Glauber [10] and recent experiments [14, 16, 17], the collective spin of an atomic gas with magnetic moments polarized opposite an applied magnetic field can be approximated as a negative-mass oscillator. The positive-mass oscillator is provided by the center-of-mass motion of the same trapped atomic gas, cooled initially near its ground state. A single-mode optical cavity introduces a third quantum element, which couples to each oscillator through magneto-optical and optomechanical interactions, respectively. This cavity field both mediates interactions between the two oscillators, leading to a collective spin-orbit coupling within the atomic gas, and facilitates continuous measurement of the hybrid system, with precision near the standard quantum limits [18]. We observe amplification of both oscillators by the negative-mass instability, which, similar to a non-degenerate parametric amplifier, induces strongly correlated excitations in both modes. We estimate the covariance of the resulting two-mode state from measurements of its transient decay during subsequent free evolution. The observed gain and correlation amplitude are described well by a linearized model of the hybrid optodynamical system.

To illustrate the negative-mass instability, consider a system of two harmonic oscillators, described by unitless bosonic operators $\hat{a}$ and $\hat{b}$, evolving at frequencies $\omega_{\mathrm{m}} = \omega_0 + \delta/2$ and $\omega_{\mathrm{s}} = \omega_0 - \delta/2$, and let ϵ represent the sign of the second oscillator's mass. If coupled by a spring of strength Ω, the resulting dynamics are described by the interaction-picture Hamiltonian

$$\mathcal{H}_I = \frac{\hbar\Omega}{2} \left(\hat{a}^\dagger \hat{b} \, e^{i(\omega_{\mathrm{m}} - \epsilon\omega_{\mathrm{s}})t} + \hat{a}^\dagger \hat{b}^\dagger e^{i(\omega_{\mathrm{m}} + \epsilon\omega_{\mathrm{s}})t} + h.c. \right). \quad (1)$$

For nearly resonant oscillators, under the rotating-wave approximation, this interaction hybridizes their dynamics into coupled normal modes with eigenfrequencies $\omega_\pm = \omega_0 \pm \sqrt{\delta^2 + \epsilon\Omega^2}/2$. For positive masses ($\epsilon = +1$), the interaction results in a familiar avoided crossing in the energy spectrum and facilitates resonant exchange of excitations [Fig. 1a], conserving the total excitation number.

However, when the mass of the second oscillator is negative ($\epsilon = -1$), the pair-creation and pair-annihilation terms of the interaction are resonant [Fig. 1b], driving amplification of both oscillators. For strong coupling ($|\Omega| > |\delta|$), the normal-mode eigenvalues become complex, indicating the onset of the negative-mass instability. In this condition, the oscillation frequencies of the normal modes, described by $\mathrm{Re}[\omega_\pm]$, synchronize, while the instability gain, described by $G_\pm = 2\,\mathrm{Im}[\omega_\pm]$, indicates
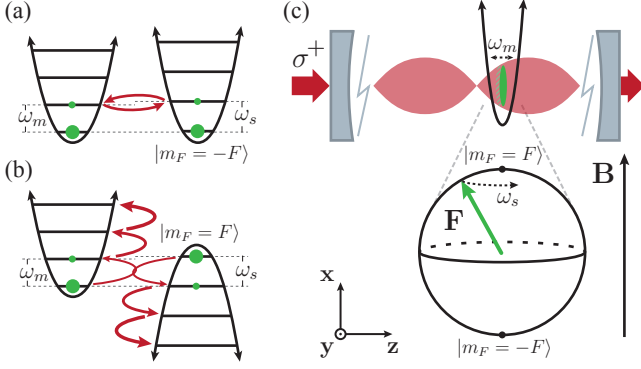
FIG. 1. (a-b) Energy levels of two nearly degenerate harmonic oscillators. (a) For positive-mass oscillators, coupling mediates exchange of excitations, conserving the total excitation number. (b) For positive- and negative-mass oscillators, the interaction resonantly drives pair creation, resulting in exponential growth of a correlated mode. (c) The center-of-mass motion of a harmonically confined, ultracold atomic ensemble (green), with trap frequency ω_{m}, represents the positive-mass oscillator. Larmor precession at frequency ω_{s} of the collective atomic spin near its highest-energy state, in an applied magnetic field $\mathbf{B} \propto \mathbf{x}$, approximates a negative-mass oscillator. Position- and spin-dependent dispersive coupling to a circularly-polarized mode of the optical cavity (red) mediates coherent interaction between the oscillators and facilitates continuous measurement of their dynamics.

exponential amplification of one mode and damping of the other [19]. For resonant coupling ($\delta = 0$), the amplified normal mode describes correlated motion of the two oscillators with a relative phase of $\pi/2$. The resulting dynamics are similar to two-mode parametric amplification observed in driven optical four-wave mixing and down-conversion [20], which gives rise to the same equations of motion in a rotating frame defined by the optical pump [21].

We experimentally realize the negative-mass instability using a gas of about 3000 ^{87}Rb atoms, cooled to about 3 μK by rf evaporation, and trapped in a single antinode of a standing-wave optical dipole trap (wavelength 842 nm), resonant with a TEM$_{00}$ mode of a high-finesse, Fabry-Pérot optical cavity [22]. For small displacements, the axial atomic motion is approximately harmonic, with trap frequency ω_{m} controlled by the dipole trap intensity, defining a positive-mass, center-of-mass mode with unitless displacement $\hat{Z}_{\mathrm{m}} = \hat{a} + \hat{a}^\dagger$ defined in terms of bosonic phonon operators.

The ensemble is initially spin-polarized in the $|f = 2, m_f = 2\rangle$ electronic ground-state, yielding a total spin $F \sim 6000$. Applying a magnetic field along $\mathbf{x}$, transverse to the cavity axis, induces Larmor precession in the $\mathbf{y}$-$\mathbf{z}$ plane at frequency ω_{s}. For small, collective excitations of the total dimensionless spin $\hat{\mathbf{F}}$ away from the magnetic field axis, the Larmor precession can be approximated as the motion of a harmonic oscillator, with unitless dis-

placement defined as $\hat{Z}_{\mathrm{s}} = \sqrt{F/2}\,\hat{F}_z = \hat{b} + \hat{b}^\dagger$ in terms of bosonic operators [23]. The effective mass of this oscillator is negative (positive) for a spin precessing near its highest-energy (lowest-energy) state [17].

The atomic ensemble is probed through its influence on another TEM$_{00}$ cavity mode, with half-linewidth $\kappa/2\pi = 1.82$ MHz, which is detuned by $\Delta_{\mathrm{ca}}/2\pi = -42$ GHz from the atomic D_2 transition, realizing an intensity- and spin-dependent dispersive coupling to circularly polarized light. Positioning the trapped ensemble at the maximum intensity gradient of the probe field [Fig. 1c], its axial motion modulates the dispersive interaction, providing linear coupling to the center-of-mass displacement $\hat{Z}_{\mathrm{m}}$. Optical coupling to the collective spin arises from the circular birefringence of the atomic ensemble [24]. For a cavity driven with circularly polarized light, this birefringence causes the dispersive coupling strength to depend linearly on $\hat{F}_z$, the projection of the total spin along the cavity axis, such that the cavity mode is coupled to one oscillating component of the transverse spin [25].

Linearizing the collective dynamics for small excitations around an average cavity photon number $\bar{n}$, in a frame rotating at the optical probe frequency ω_{p}, results in an effective Hamiltonian [26]

$$
\begin{aligned}
\mathcal{H} = {} & \hbar\omega_{\mathrm{m}}\hat{a}^\dagger\hat{a} + \epsilon\hbar\omega_{\mathrm{s}}\hat{b}^\dagger\hat{b} - \hbar\Delta_{\mathrm{pc}}\hat{c}^\dagger\hat{c} \\
& + \hbar\sqrt{\bar{n}}(\hat{c} + \hat{c}^\dagger)\left[g_{\mathrm{m}}\hat{Z}_{\mathrm{m}} + g_{\mathrm{s}}\hat{Z}_{\mathrm{s}}\right] + \hbar\bar{n}g_{\mathrm{sm}}\hat{Z}_{\mathrm{m}}\hat{Z}_{\mathrm{s}}, \quad (2)
\end{aligned}
$$

where $\Delta_{\mathrm{pc}} = \omega_{\mathrm{p}} - \omega_{\mathrm{c}}$ is the probe detuning from cavity resonance, $\hat{c}$ is the annihilation operator for photons in the cavity mode, and $\epsilon = -\mathrm{sgn}\langle\hat{F}_x\rangle$ is the sign of the spin oscillator's effective mass. The coupling rates defined here are $g_{\mathrm{s}}/2\pi = -18$ kHz, $g_{\mathrm{m}}/2\pi = 26$ kHz, and $g_{\mathrm{sm}}/2\pi = 120$ Hz for our system.

The coherent interactions between the three modes described by this Hamiltonian are more complicated than the model introduced in Eq. 1. However, the two-mode model can be recovered by adiabatic elimination of the cavity mode, in the unresolved sideband regime ($\kappa \gg \omega_{\mathrm{m}}, \omega_{\mathrm{s}}$). This results in optodynamical coupling between the collective motion and spin, with strength $\Omega_{\mathrm{opt}} = 4g_{\mathrm{s}}g_{\mathrm{m}}\bar{n}\Delta_{\mathrm{pc}}/(\kappa^2 + \Delta_{\mathrm{pc}}^2)$ [28], in addition to independent optodynamical frequency shifts [29, 30] and damping [31–33] of each oscillator.

The final term of Eq. 2 describes an additional, direct interaction between the motion and spin, which depends only on the mean photon number $\bar{n}$. This 'static' interaction arises from the spatial variation of the vector Stark shift and couples the motion and spin of each atom. Eq. 2 captures the projection of this interaction onto the collective modes, which, combined with the optodynamical coupling, results in a net spring strength $\Omega = \Omega_{\mathrm{opt}} + 2\bar{n}g_{\mathrm{sm}}$. In addition, there are residual incoherent dynamics, due to weak coupling between the spin
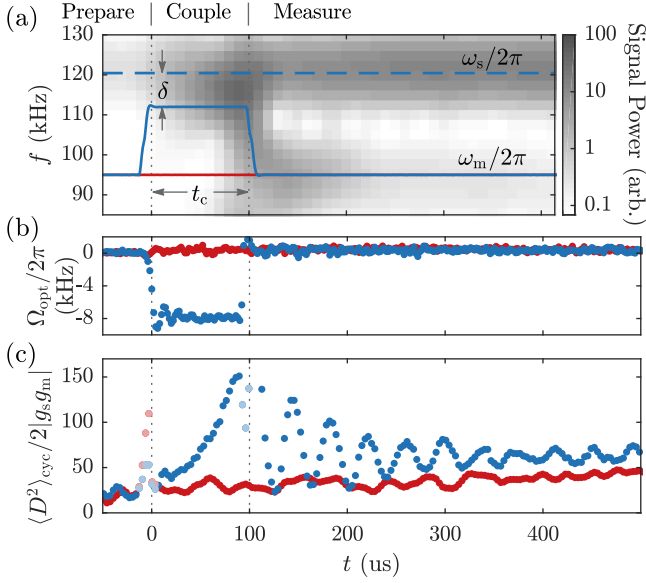
FIG. 2. Observation of negative-mass instability. (a) Spectrogram of total optical modulation observed during the experimental sequence, averaged over 200 iterations. The spectrum shows components at the Larmor frequency, fixed at $\omega_s = 120$ kHz (dashed line), and the mechanical frequency, initially at $\omega_m = 95$ kHz then varied during coupling to achieve the desired detuning (solid line). The collective spin shows negligible decay and the motion damps at rate $\Gamma_m/2\pi = 2$ kHz. (b) Optodynamical coupling strength Ω_{opt}, calculated from the measured Δ_{pc} and $\bar{n}$. Experiments are performed with a coupling pulse with average $\bar{n} = 15$ and $\Delta_{\mathrm{pc}} = 1.4$ MHz (blue) and without coupling (red). (c) The mean squared joint displacement of both oscillators, captured in the cycle-averaged optical modulation power between 85 kHz and 150 kHz. This signal reflects exponential amplification of both oscillators while coupled, followed by a stationary beat during the subsequent free evolution, revealing the transient decay of correlations created between the two modes. Transients from changes in the optical probe and trap intensity perturb measurements near $t = 0$ and $t = t_c$ (light points), which are excluded from analysis.

and the thermal motion of each atom in the center-of-mass frame, which mediate a resonant, incoherent transfer of energy from the initially polarized spin into the mechanical bath, resulting in loss of spin polarization and anomalous diffusion of its precession [26].

Owing to the spin- and position-dependent dispersive coupling in Eq. 2, the probe field is sensitive to the joint displacement operator $\hat{D} = g_m \hat{Z}_m + g_s \hat{Z}_s$, imparting a state-dependent frequency shift to the effective cavity resonance. Through this shift, the oscillator dynamics are imprinted on phase and amplitude modulation of light transmitted through the cavity. These modulations are observed using an optical heterodyne detector, with total cavity photon detection efficiency $\varepsilon = 9\%$, from which a measurement record of $\hat{D}$ is recovered.

We observe the negative-mass instability by applying a short optical coupling pulse to initially uncorrelated oscillators and measuring the subsequent free ringdown of the resulting state [Fig. 2]. During the initial preparation, the oscillator frequencies are well resolved to suppress interactions while the probe is stabilized on cavity resonance ($\Delta_{\mathrm{pc}} = 0$) at a minimal intensity ($\bar{n} \approx 1$ [34]). In the final stage of preparation, the mechanical frequency ω_m is adiabatically ramped in 10 μs to achieve the desired detuning from the Larmor frequency $\delta = \omega_m - \omega_s$ [Fig. 2a]. The optical interaction is then quickly turned on for coupling time t_c by increasing the probe intensity and stepping its detuning Δ_{pc} to achieve the desired coupling strength [Fig. 2b]. To observe the transient decay of the correlated two-mode state after the coupling pulse, the probe intensity is reduced ($\bar{n} \approx 4$), for improved measurement sensitivity, and the oscillator frequencies are resolved, by adiabatically ramping the optical trap back to its initial depth in 10 μs.

The coupled system evolves according to the projection of the oscillator's initial states onto the hybrid normal modes, where, under strong coupling, one mode is amplified and the other is damped. Because both oscillators start near their ground states, without well-defined phases, the absolute phase of the amplified mode is random. Therefore, each oscillator, observed independently, is driven into an effective thermal state with increased mean occupation, and the observed joint displacement $\langle \hat{D} \rangle$ averages to zero. However, the growth of correlation between the oscillators results in motion with a fixed relative phase.

Both the amplification and correlation generated by the negative-mass instability are clearly captured in the cycle-averaged mean squared joint displacement

$$\langle \hat{D}^2 \rangle_{\mathrm{cyc}} = g_m^2 \langle 2\hat{a}^\dagger \hat{a} + 1 \rangle + g_s^2 \langle 2\hat{b}^\dagger \hat{b} + 1 \rangle + 4g_m g_s \langle \mathrm{Re}[\hat{a}\,\hat{b}] \rangle.$$

Time evolution of this signal reveals the exponential growth of both oscillators during coupling, in addition to a stationary beat due to interference of the resulting two-mode correlations during subsequent free evolution [Fig. 2c]. This beat represents a self-heterodyne measurement arising from the product of the oscillator amplitudes, which evolves at their frequency difference, with initial amplitude and phase reflecting the magnitude and phase of correlation in the final state.

The instability gain is measured in two ways—from growth of $\langle \hat{D}^2 \rangle_{\mathrm{cyc}}$ observed during coupling and from estimates of the resulting two-mode state after variable t_c. Under strong coupling, both normal modes evolve at approximately the same frequency, such that $\langle \hat{D}^2 \rangle_{\mathrm{cyc}}$ predominately displays exponential growth at rate G_+, while incoherent dynamics driven by the thermal mechanical bath add diffusive growth to the observed signal. For sufficiently strong optical coupling Ω, near the optimal probe detuning $|\Delta_{\mathrm{pc}}| = \kappa$, the coherent interaction is dominant, resulting in the onset of instability observed
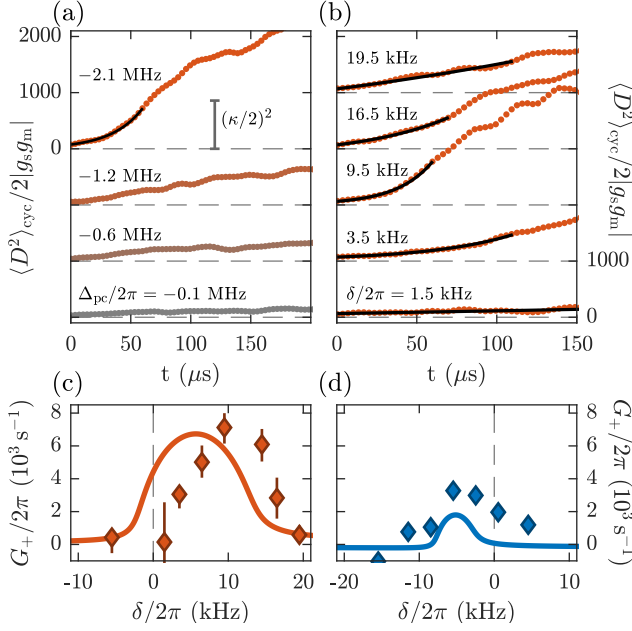
FIG. 3. (a) Onset of instability, observed in the mean squared displacement, for increasing optical coupling strength, with $\bar{n} = 10$ and oscillator detuning $\delta/2\pi = 14$ kHz. Each trace (offset for clarity) is the average of around 30 repetitions. Growth saturates due to the finite cavity linewidth (scale bar) and other non-linearities. (b) Resonance of instability for varied δ, under strongest optical coupling in (a). The instability gain G_+ is extracted by least-square fits (lines) to data at early times. (c) G_+ (red diamonds) versus δ, compared to predicted steady-state gain (solid line). The peak instability occurs at finite detuning, due to optodynamical shifts of each oscillator's frequency. The larger frequency shift observed might be due to asymmetric transients, not reflected in the theoretical steady-state gain. (d) For an inverted probe detuning ($\Delta_{\mathrm{pc}} = +2.0$ MHz), the optodynamical coupling acts opposite the static coupling, resulting in reduced peak gain (blue diamonds). Error bars in (c-d) represent combined 1-σ statistical uncertainty from the fit and systematic error estimated from $\pm 10\%$ variations of the fit interval.
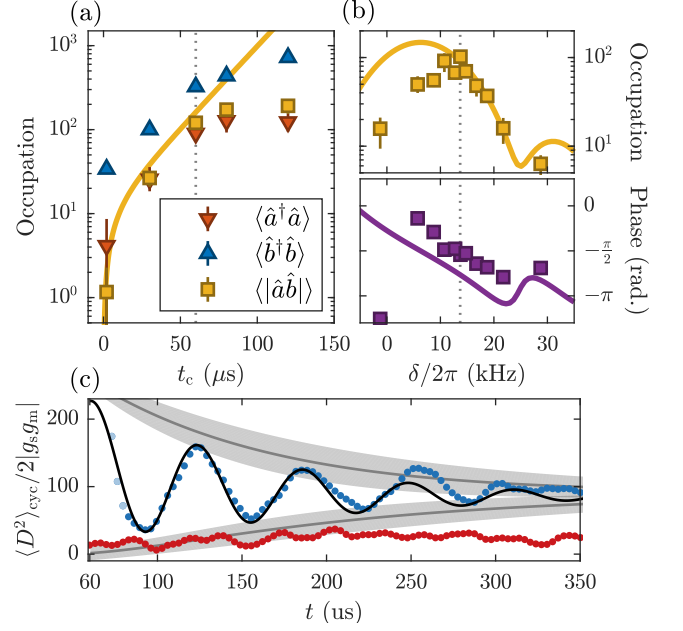
FIG. 4. Results of matched-filter analysis. (a) Growth of the mechanical (red downward triangle), spin (blue upward triangle), and correlated (yellow squares) occupation as a function of t_{c}, with $\delta/2\pi = 14$ kHz and the same optical coupling as Fig. 3c. The observed correlated occupation agrees well with the predicted evolution of the measured initial state at the optimal detuning (yellow line). Growth saturates near a mechanical occupation of 100, possibly due to mechanical non-linearity of the dipole trap. (b) Correlated occupation and phase versus δ, after fixed $t_{\mathrm{c}} = 60$ μs. Error bars in (a-b) indicate combined 1-σ statistical uncertainty after 200 repetitions and estimated systematic error from the uncertainties of all filter parameters. The anomalous frequency shift is similar to that seen in Fig. 3c-d. (c) Example agreement between the beat observed in $\langle \hat{D}^2 \rangle_{\mathrm{cyc}}$ (blue points) and a simulated signal constructed from time-evolution of the estimated two-mode state (black line). Shaded regions show 1-σ bounds for evolution of a maximally-correlated state with the same estimated individual oscillator occupations. Similar measurements performed without coupling (red points) show evolution of the initial state.

in exponential growth of $\langle \hat{D}^2 \rangle_{\mathrm{cyc}}$ [Fig. 3a]. The instability quickly drives the system into saturation, but for early times, the coherent growth is clearly reflected in the curvature of the measured signal.

We explore the instability's resonance by repeating these measurements over a range of δ [Fig. 3b]. The instability gain is extracted from the signal by a least-squares fit to a model describing coherent exponential amplification with additional diffusive noise, using independent rates to distinguish the coherent and incoherent dynamics [26]. The peak instability occurs at a non-zero detuning [Fig. 3c], because independent optodynamical frequency shifts act on each oscillator in opposite directions, shifting them into resonance. Inverting the sign of optical coupling Ω_{opt}, with an equal but opposite Δ_{pc}, reveals the effect of the static coupling as an asymmetry in the observed gain [Fig. 3d].

The mean squared displacement, however, lacks spectral information distinguishing the occupation of each oscillator. To estimate the final two-mode state $\hat{\mathbf{v}} = (\hat{a}^\dagger \ \hat{b})^T$ from each experimental iteration, we apply linear matched filters directly to the free ringdown observed after the coupling pulse, extracting single-shot estimates for the amplitude and phase of each oscillator [28, 35]. From an ensemble of measurements, we estimate the second-moment matrix $\mathbf{C} = \langle \hat{\mathbf{v}} \hat{\mathbf{v}}^\dagger \rangle$, correcting for correlated contributions from thermal noise, measurement backaction, and detector shot-noise during the measurement interval [26].

The diagonal components of the Hermitian matrix $\mathbf{C}$ capture the exponential growth of each oscillator's occupation for increasing t_{c}. The off-diagonal component

describes the amplitude and phase of correlation in the resulting state, which demonstrates the strong correlation of excitations added to both oscillators, providing an independent measure of G_+ unperturbed by the incoherent dynamics [Fig. 4a]. This amplitude and phase is measured across a range of δ, for a fixed $t_c = 60$ μs, revealing the resonance of the correlation growth, with the expected correlation phase $\phi = -\pi/2$ at the optimal detuning [Fig. 4b]. We verify these matched-filter results by reconstructing the mean squared displacement from time evolution of the estimated covariance matrix C [Fig. 4c].

In conclusion, we have demonstrated cavity-mediated coupling of the collective spin and motion of a trapped atomic ensemble. For a high-energy polarized spin, this interaction results in a negative-mass instability, with dynamics analogous to a self-driven parametric amplifier. We observed coherent amplification of a correlated mode by the instability, using time-resolved matched-filter analysis to estimate the covariance of the two-mode correlated state. This instability could be applied as a coherent amplifier of an optomechanical state, facilitating enhanced measurement sensitivity, or to generate two-mode squeezed states, for use in entanglement enhanced metrology. While, in our present system, any potential squeezing is obscured by incoherent coupling to thermal motion, this limitation could be avoided by using separate spin and mechanical oscillators, coupled only by cavity optodynamics.

---

* jkohler@berkeley.edu

† dmsk@berkeley.edu

[1] N. W. Ashcroft and N. D. Mermin, *Solid state physics* (Saunders, New York, 1976) p. 826.

[2] C. E. Nielsen, A. M. Sessler, and K. R. Symon, in *2nd Int. Conf. High-Energy Accel. Instrum.*, edited by L. Kowarski (CERN, Geneva, Switzerland, 1959) pp. 239–252.

[3] A. A. Kolomenskii and A. N. Lebedev, J. Nucl. Energy. Part C, Plasma Physics, Accel. Thermonucl. Res. **3**, 44 (1961).

[4] M. A. H. Tucker and A. F. G. Wyatt, Science **283** (1999).

[5] B. Eiermann, P. Treutlein, T. Anker, M. Albiez, M. Taglieber, K.-P. Marzlin, and M. K. Oberthaler, Phys. Rev. Lett. **91**, 060402 (2003).

[6] M. A. Khamehchi, K. Hossain, M. E. Mossman, Y. Zhang, T. Busch, M. M. Forbes, and P. Engels, Phys. Rev. Lett. **118**, 155301 (2017).

[7] H. Postma, J. L. Dunlap, R. A. Dory, G. R. Haste, and R. A. Young, Phys. Rev. Lett. **16**, 265 (1966).

[8] D. Strasser, T. Geyer, H. B. Pedersen, O. Heber, S. Goldberg, B. Amarant, A. Diner, Y. Rudich, I. Sagi, M. Rappaport, D. J. Tannor, and D. Zajfman, Phys. Rev. Lett. **89**, 283204 (2002).

[9] R. V. E. Lovelace and R. G. Hohlfeld, Astrophys. J. **221**, 51 (1978).

[10] R. J. Glauber, Ann. N. Y. Acad. Sci. **480**, 336 (1986).

[11] K. Hammerer, M. Aspelmeyer, E. S. Polzik, and P. Zoller, Phys. Rev. Lett. **102**, 020501 (2009).

[12] M. Tsang and C. M. Caves, Phys. Rev. Lett. **105**, 123601 (2010).

[13] C. F. Ockeloen-Korppi, E. Damskägg, J.-M. Pirkkalainen, A. A. Clerk, M. J. Woolley, and M. A. Sillanpää, Phys. Rev. Lett. **117**, 140401 (2016).

[14] C. B. Møller, R. A. Thomas, G. Vasilakis, E. Zeuthen, Y. Tsaturyan, M. Balabas, K. Jensen, A. Schliesser, K. Hammerer, and E. S. Polzik, Nature **547**, 191 (2017).

[15] C. K. Andersen and K. Mølmer, Phys. Rev. A **86**, 043831 (2012).

[16] H. Krauter, C. A. Muschik, K. Jensen, W. Wasilewski, J. M. Petersen, J. I. Cirac, and E. S. Polzik, Phys. Rev. Lett. **107**, 080503 (2011).

[17] J. Kohler, N. Spethmann, S. Schreppler, and D. M. Stamper-Kurn, Phys. Rev. Lett. **118**, 063604 (2017).

[18] S. Schreppler, N. Spethmann, N. Brahms, T. Botter, M. Barrios, and D. M. Stamper-Kurn, Science **344**, 1486 (2014).

[19] A. Gloppe, P. Verlot, E. Dupont-Ferrier, A. Siria, P. Poncharal, G. Bachelier, P. Vincent, and O. Arcizet, Nat. Nanotechnol. **9**, 920 (2014).

[20] A. S. Lane, M. D. Reid, and D. F. Walls, Phys. Rev. A **38**, 788 (1988).

[21] L. Buchmann and D. M. Stamper-Kurn, Phys. Rev. A **92**, 013851 (2015).

[22] T. P. Purdy, D. W. C. Brooks, T. Botter, N. Brahms, Z.-Y. Ma, and D. M. Stamper-Kurn, Phys. Rev. Lett. **105**, 133602 (2010).

[23] T. Holstein and H. Primakoff, Phys. Rev. **58**, 1098 (1940).

[24] W. Happer and B. S. Mathur, Phys. Rev. Lett. **18**, 577 (1967).

[25] N. Brahms and D. M. Stamper-Kurn, Phys. Rev. A **82**, 041804 (2010).

[26] See Supplemental Material at [SMURL], which includes Ref. [27], for a derivation of the linearized Hamiltonian, and description of the instability fit procedure and matched filter analysis.

[27] N. Brahms, T. Botter, S. Schreppler, D. W. C. Brooks, and D. M. Stamper-Kurn, Phys. Rev. Lett. **108**, 133601 (2012).

[28] N. Spethmann, J. Kohler, S. Schreppler, L. Buchmann, and D. M. Stamper-Kurn, Nat. Phys. **12**, 27 (2015).

[29] B. S. Sheard, M. B. Gray, C. M. Mow-Lowry, D. E. McClelland, and S. E. Whitcomb, Phys. Rev. A **69**, 051801 (2004).

[30] T. Corbitt, D. Ottaway, E. Innerhofer, J. Pelc, and N. Mavalvala, Phys. Rev. A **74**, 021802 (2006).

[31] O. Arcizet, P.-F. Cohadon, T. Briant, M. Pinard, and A. Heidmann, Nature (London) **444**, 71 (2006).

[32] S. Gigan, H. R. Böhm, M. Paternostro, F. Blaser, G. Langer, J. B. Hertzberg, K. C. Schwab, D. Bäuerle, M. Aspelmeyer, and A. Zeilinger, Nature (London) **444**, 67 (2006).

[33] A. Schliesser, P. Del'Haye, N. Nooshi, K. J. Vahala, and T. J. Kippenberg, Phys. Rev. Lett. **97**, 243905 (2006).

[34] This probe intensity is chosen to minimize diffusion of the collective spin from coupling to thermal motion and accumulated measurement backaction, while providing sufficient signal-to-noise for the cavity-probe detuning feedback.

[35] T. A. Palomaki, J. D. Teufel, R. W. Simmonds, and K. W. Lehnert, Science **342**, 710 (2013).